Journal of Power Sources 188 (2009) 404–410

Contents lists available at ScienceDirect

Journal of Power Sources

journal homepage: www.elsevier.com/locate/jpowsour

Enhanced electrochemical hydrogen storage by catalytic Fe-doped multi-walled carbon nanotubes synthesized by thermal chemical vapor deposition

A. Reyhani [a], S.Z. Mortazavi [b], A.Z. Moshfegh [a,c,*], A. Nozad Golikand [b], M. Amiri [a]

[a] Department of Physics, Sharif University of Technology, P.O. Box 11155-9161, Tehran, Iran
[b] Institute of Materials, P.O. Box 31485-498, Karaj, Iran
[c] Institute for Nanoscience and Nanotechnology, Sharif University of Technology, P.O. Box 14588-8969, Tehran, Iran

ARTICLE INFO

Article history:
Received 17 June 2008
Accepted 29 November 2008
Available online 7 December 2008

Keywords:
Hydrogen storage
Electrochemical
TCVD
Fe-doped MWCNTs

ABSTRACT

Hydrogen storage capacities of raw, oxidized, purified and Fe-doped multi-walled carbon nanotubes (MWCNTs) were studied by electrochemical method. Based on transmission electron microscopy and Raman spectroscopic data, thermal oxidation removed defective graphite shells at the outer walls of MWCNTs. The analysis results indicated that the acid treatment dissolved most of the catalysts and opened some tips of the MWCNTs. Thermal gravimetric analysis and differential scanning calorimetry results illustrated that by oxidation and purification of MWCNTs, the weight loss peak shifts toward a higher temperature. N_2 adsorption isotherms of the purified and oxidized MWCNTs showed an increase in N_2 adsorption below $P/P_o = 0.05$, suggesting that microporous structures exist in the purified and oxidized MWCNTs. The electrochemical results revealed that the Fe-doped MWCNTs produced the highest hydrogen storage capacities compared to the other samples in various sweep rates. According to electrochemical analyses, the peak currents of hydrogen adsorption/desorption increased by increasing the catalyst's active surface.

1. Introduction

Nowadays, hydrogen is recognized as an ideal fuel for energy conversion because of high efficiency and its role in the reduction of air pollution [1]. However, due to the existence of major scientific challenges, it has not been so far used in great extent. Further, developing a safe, effective and cheap hydrogen storage system is the main challenge [2–4]. To date, different methods of hydrogen storage have been applied but none of them have completely satisfied the proposed standard by the US Department of Energy (DOE) [2]. Therefore, in order to obtain a high efficient hydrogen storage, new porous materials such as carbon nanotubes (CNTs), carbon nanofibers and active carbons have been considered for this purpose [1,2,5]. Since the report of Dillon et al. [6] on a possible 5–10% hydrogen storage capacity for single-walled carbon nanotubes (SWCNTs) due to their better electrical property, small density, high porosity and high active surface area for hydrogen adsorption, CNTs have attracted much attention in new porous materials for safer hydrogen storage.

It has been widely reported that growth [7], synthesis conditions [8], structure [9–12], purification [13] and functionalization [14] of CNTs have a strong effect on hydrogen storage capacity. Yi et al. [15] investigated the effect of multi-walled carbon nanotubes (MWCNTs) on electrochemical properties of Ni-CNTs treated with different temperatures under nitrogen ambient and showed that the Ni-CNTs treated at 800 °C have a better hydrogen storage property as compared with other temperatures. Fazle Kibria et al. [7] investigated the hydrogen storage behavior of undoped CNTs as well as Li-, Na-, and K-doped CNTs by electrochemical method and found that metal-doped CNTs stored higher amounts of hydrogen than the undoped CNTs. Feng et al. [16] showed that the amount of MWCNTs of Ni-MWCNT electrode prepared by composite electro-deposition method can be up to 22.45% for hydrogen storage. Hsieh et al. [17] in an investigation on the electrochemical hydrogen storage characteristics of Ni-doped CNTs found that the specific current for hydrogen storage increases with the increasing of Ni loading. Lombardi et al. [18] found that vacuum annealing (950 °C, 1 h) decreased the electrochemical hydrogen storage capacities of the MWCNTs purified by nitric acid.

There are many methods for the growth of CNTs but thermal chemical vapor deposition (TCVD) has many advantages in that it allows CNTs to be synthesized with high purity, high yield, selective growth and low cost [10,11]. Among the many supports and catalysts for the growth of CNTs by TCVD, MgO as support [19,20] and

* Corresponding author at: Department of Physics, Sharif University of Technology, P.O. Box 11155-9161, Tehran, Iran. Tel.: +98 21 6600 5410; fax: +98 21 6601 2983.
E-mail address: moshfegh@sharif.edu (A.Z. Moshfegh).

0378-7753/$ – see front matter © 2008 Elsevier B.V. All rights reserved.
doi:10.1016/j.jpowsour.2008.11.131

bimetallic systems of transition metals as catalyst [21–26] produce higher yield CNTs.

The present study aimed at investigating and comparing the effects of oxidation, purification and doping of Fe on the electrochemical hydrogen storage capacities of MWCNTs. Scanning electron microscopy (SEM), transmission electron microscopy (TEM), X-ray diffraction (XRD), X-ray photoelectron spectroscopy (XPS), thermal gravimetric analysis (TGA), differential scanning calorimetry (DSC), Brunauer–Emmett–Teller (BET), Barret–Joyner–Halenda (BJH) and Raman spectroscopy techniques were used to evaluate the size, structure, graphitization, yield, quality and adsorption characteristics of the raw, oxidized, purified and Fe-doped MWCNTs. In addition, cyclic voltammetry and chronopotentiometry were used to determine the electrochemical characteristics of the samples.

2. Experimental

2.1. Catalyst preparation

Bimetallic catalyst of Fe and Ni supported by MgO (with the proportion of 1:1:8) was prepared using a wet chemical impregnation method as follows:

One gram of MgO powder (99.9%–Merck) was dispersed in 20 ml of distilled water and the obtained suspension was sonicated for 30 min in order to get a homogeneous solution. Then, appropriate amounts of metal nitrates (Fe $(NO_3)_3{\cdot}9H_2O$ and Ni $(NO_3)_2{\cdot}6H_2O$) were added to the MgO suspension and the mixture was stirred for 30 min. The prepared impregnate was dried in an oven at 150 °C for 24 h in air. After drying, the mixture was ground to fine powder as catalyst.

2.2. MWCNT growth

After preparation of the catalyst, the sample was loaded into a quartz tubular furnace at the atmospheric pressure. The furnace temperature was ramped from the room temperature to 700 °C in Ar flow (80 sccm) for 40 min. Then, a mixture of Ar (20 sccm) and H_2 (60 sccm) was fed into the furnace. When the temperature stabilized at 900 °C, the mixture flow was stopped and NH_3 (80 sccm) was introduced into the furnace at the same temperature for 40 min. Then, temperature of the furnace was ramped to 940 °C in 10 min under H_2 flow at 80 sccm. When the temperature stabilized at 940 °C, high purity CH_4 gas was introduced into the furnace at a flow of 80 sccm for 40 min. Finally, Ar gas (80 sccm) was reintroduced into the furnace for cooling.

2.3. Purification and functionalization of MWCNTs

Purification of the grown MWCNTs was performed within two steps. Initially, the MWCNTs were heated in a furnace at 450 °C for 60 min in O_2 ambient (step 1). Then, they were immersed in 0.1 M nitric acid solution for 4 h at 100 °C (step 2). The obtained MWCNTs were washed out several times with deionized water until the pH value of the solution became neutral. The sample was then dried at 150 °C for 24 h.

For functionalization of the MWCNTs, 30 mg of the purified MWCNTs and 1 g of Fe nitrate were immersed in distilled water and the mixture was stirred at 50 °C for 1 h. Then, the ionic-adsorbed MWCNTs were separated from the Fe salt solution using a filtration. The obtained Fe-doped MWCNTs were heated at 200 °C for 24 h.

2.4. Sample characterization

Characterization of the samples was carried out by the following techniques: SEM (Philips XL30) was used to determine morphology and average diameter of the MWCNTs. TEM (Philips XL) was carried out for the accurate determination of diameter, shape and microstructure of the MWCNTs. For TEM analysis, the samples were prepared with dispersion of the MWCNTs in acetone using an ultrasonic bath. Then, one drop of the prepared suspension was deposited on a carbon coated copper grid. Raman spectroscopy (HR-800 Jobin-Yvon) was utilized to determine the quality of the MWCNTs. The Raman spectra were recorded from 200 to 2000 cm^{-1}. Structure and graphitization degree of the MWCNTs were characterized by XRD using Cu Kα radiation source ($\lambda = 1.541$ Å). The scanning speed and step interval were 1° and 0.02° min^{-1}, respectively. TGA and DSC techniques were employed to investigate the yield and graphitization of MWCNTs using Rometric simultaneous thermal analysis (STA). The heating program was considered in a temperature range of 30–850 °C with the heating rate of 10 °C min^{-1} in air ambient. A high-performance volumetric physisorption apparatus at 77 K (BET) was used to determine the effective surface area of the MWCNTs. Pore size distribution of the MWCNTs was also obtained by BJH equation using the adsorption

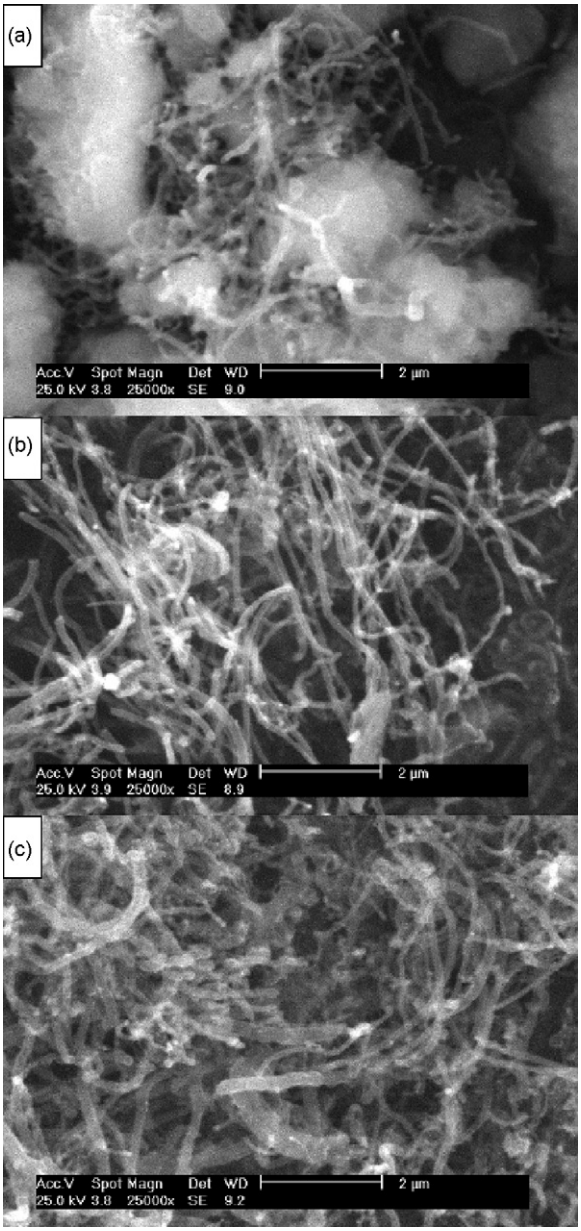

Fig. 1. SEM micrographs of the (a) raw, (b) oxidized and (c) purified MWCNTs.

isotherm. Chemical composition of the MWCNTs was determined by XPS using Al Kα radiation source with the incident energy of 1486.6 eV.

2.5. Electrode preparation and electrochemical measurements

The raw, oxidized, purified and Fe-doped MWCNTs were used to fabricate the electrodes as follows:

Two milligram of the MWCNTs was added into a solution of nafion (0.1 ml) and deionized water (3 ml). Then, the obtained solution was sonicated for 30 min. A stainless steel plate (20 mm × 30 mm × 1 mm) was used as the cathode matrix. After burnishing, it was corroded in a HF solution (30%) for 20 min. Then, the sonicated solution of MWCNTs was poured dropwise on the porous stainless steel plate. Finally, the electrodes were dried in an oven at 80 °C for 2 h.

Electrochemical hydrogen storage capacities of the MWCNTs were studied using a three-electrode system (Auto lab 302) at ambient temperature in 6 M solution of NaOH as the electrolyte. A Ni wire as the counter electrode and an Ag/AgCl as the reference electrode were used. Cyclic voltammetric (CV) measurements of the prepared MWCNT electrodes were done in a potential range of −1.5 to 0.5 V with six sweep rates of 5, 10, 20, 30, 50, 100 mv s^{-1}. The experiments of charging/discharging were carried out under the following conditions:

The electrodes were charged for 30 min in a constant current of 5 mA and discharged under the same constant current.

3. Results and discussion

3.1. Characterization of the MWCNTs

Fig. 1 shows the SEM micrographs of the raw, oxidized (step 1) and purified (step 2) MWCNTs. According to SEM analysis, the MWCNTs have various lengths and diameters. Fig. 1(a) shows the presence of impurities in the samples and Fig. 1(b) demonstrates the decreasing of the impurities after annealing at 450 °C in O_2 ambient for 1 h. After purification (Fig. 1(c)), the support materials containing metal nanoparticles were substantially removed. Similar observations have recently been reported by other researchers [13,14].

The TEM images of the raw, oxidized, purified and Fe-doped MWCNTs are displayed in Fig. 2. It is clear that the raw MWCNTs consist of encapsulated tips with metal catalysts and defective graphite sheets at the outer wall surfaces. Fig. 2(b) demonstrates that defective graphite sheets were removed after annealing of the MWCNTs at 450 °C in O_2 ambient for 1 h. According to our SEM and TEM observations, the impurities such as MgO support and metal nanoparticles decreased after purification of the MWCNTs (Figs. 1c and 2c). It is clearly seen that the MWCNTs have bamboo

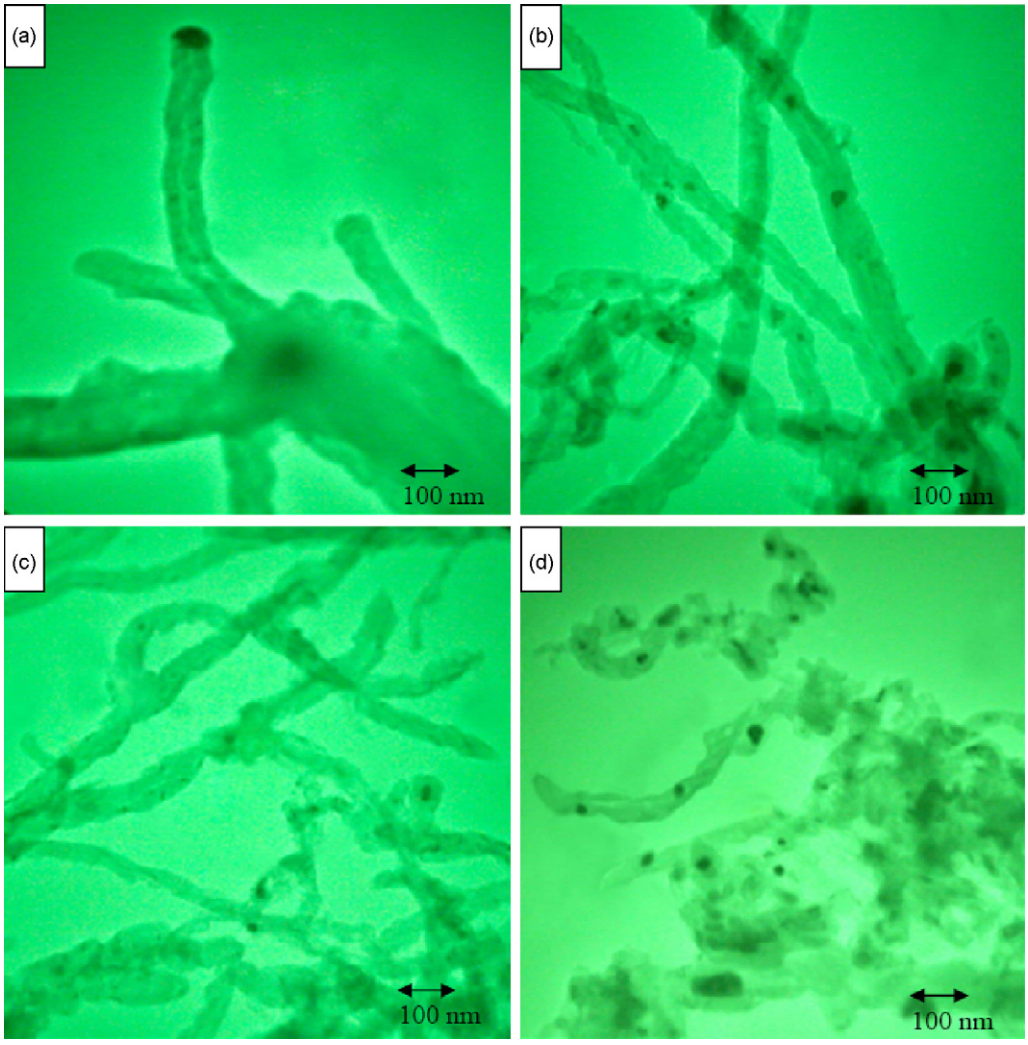

Fig. 2. TEM micrographs of the (a) raw, (b) oxidized (c) purified and (d) Fe-doped MWCNTs.

Table 1
TGA, DSC, Raman spectroscopy and XPS results of the raw, oxidized, purified and Fe-doped MWCNTs.

MWCNT samples	I_G/I_D of Raman spectra	STA results		XPS results				
		Onset, inflection and offset temperatures (°C)	Weight loss (%)	C (%)	O (%)	Mg (%)	Fe (%)	Ni (%)
Raw	1.4	520, 629 and 700	44.7	–	–	–	–	–
Oxidized	2.5	542, 641 and 700	41	74	24.6	1.4	0	0
Purified	2.2	570, 669 and 700	93	–	–	–	–	–
Fe-doped	2.1	548, 651 and 700	81	79	19.7	0	1.3	0

like structure and the outer diameters of the raw, oxidized and purified MWCNTs are about 80–150, 50–130 and 20–80 nm, respectively (Fig. 2). Further, Fig. 2(d) shows that Fe nanoparticles are attached to the MWCNTs with the average diameter of about 50 nm.

Raman spectroscopy was used to determine the quality of the MWCNTs. Table 1 shows a summary of the results obtained from Raman spectra for the raw, oxidized, purified and Fe-doped MWCNTs. The Raman bands appearing in 1500–1605 and 1250–1450 cm^{-1} of the spectrum are known as G (graphitic) and D (disorder) bands, respectively. The G band is related to the C–C band vibration frequency of the carbon material with a sp^2 orbital structure and the D band is attributed to the disorder-induced vibration of the C–C band [27]. I_G/I_D, intensity ratio of the peaks, is used as a rough measure of the sample quality [28]. This ratio is a relative response of the graphitic carbons to the defective carbons originated from the intrinsic defects in the CNTs or the amorphous carbons located on the CNTs. The I_G/I_D of the raw, oxidized, purified and Fe-doped MWCNTs was 1.4, 2.5, 2.2 and 2.1, respectively. These results implied that defective sheets decreased after both oxidation and purification. The decrease in the quality of the purified MWCNTs as compared with the oxidized MWCNTs indicates that the acid treatment destroyed some structures of the MWCNTs.

TGA and DSC curves derived from STA were used to determine the yield and the graphitization degree of MWCNTs. The yield of MWCNTs was obtained using their weight loss (%) in a temperature range of 500–800 °C. TGA and DSC results of the raw, oxidized, purified and Fe-doped MWCNTs are shown in Table 1.

The measured low weight loss for the raw MWCNTs in the temperature range of 300–400 °C indicates that almost no amorphous carbon existed in the raw MWCNTs. Also, the high yield of the purified MWCNTs (93%) shows that the acid treatment decreased catalyst particles and MgO support in the sample. These results were also confirmed by our TEM micrographs. The DSC results in Table 1 illustrate that the weight loss peak shifts toward a higher temperature during the oxidation and purification of the MWCNTs. However, for the Fe-doped MWCNTs, the oxidation started at lower temperature because the oxidation of MWCNTs is catalyzed by Fe doping as compared with the purified MWCNTs. Yoo et al. reported a similar phenomenon by using La catalyst [29]. The higher inflection temperature and the smaller difference between the onset and offset temperatures in the DSC analysis indicate that the oxidized and purified MWCNTs have better graphitization properties compared to the raw MWCNTs [25]. This result was confirmed by Raman spectra and TEM analyses. The weight loss (%) of different MWCNTs was listed in Table 1. Comparison of the purified and Fe-doped MWCNTs showed that the amount of Fe nanoparticles attached to the MWCNTs was about 12%.

The XRD results of the raw, oxidized, purified and Fe-doped MWCNTs are shown in Fig. 3. Presence of a peak at around $2\theta = 26.30°$ is characteristic of the formation of MWCNTs. The peaks at $2\theta = 38.14°$ and 77.90° indicate the presence of Fe_3C. In addition, the peaks at $2\theta = 37.02°$, 42.93° and 62.35° are characteristic of the presence of MgO. Moreover, the peaks at $2\theta = 43.86°$ and 51.05° are indicative of Fe–Ni alloy formation and the peak at $2\theta = 82.50°$ indicates the presence of Fe. Investigation of the XRD results in Fig. 3 shows that the intensity of graphite peak (0 0 2) increases by both oxidation and purification. These results were confirmed by our TEM, DSC and Raman spectroscopy analyses. Fig. 3(c) shows that the MgO peaks were removed in the nitric acid treated MWCNTs. Also, the intensity ratio of Fe–Ni peak to the graphite peak of the purified MWCNTs decreased compared to the raw and oxidized MWCNTs.

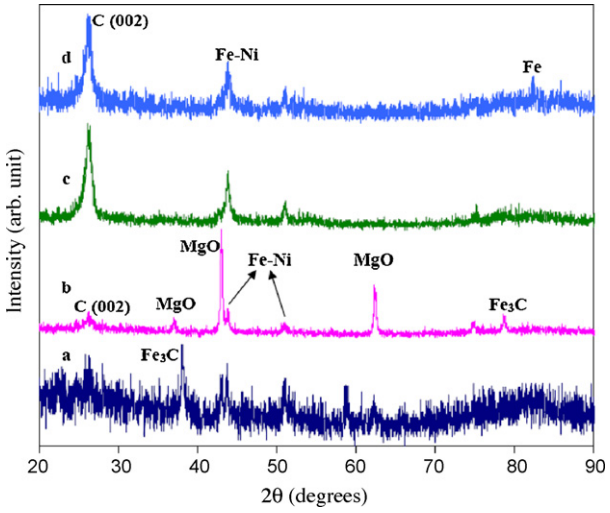

Fig. 3. XRD results of the (a) raw, (b) oxidized (c) purified and (d) Fe-doped MWCNTs.

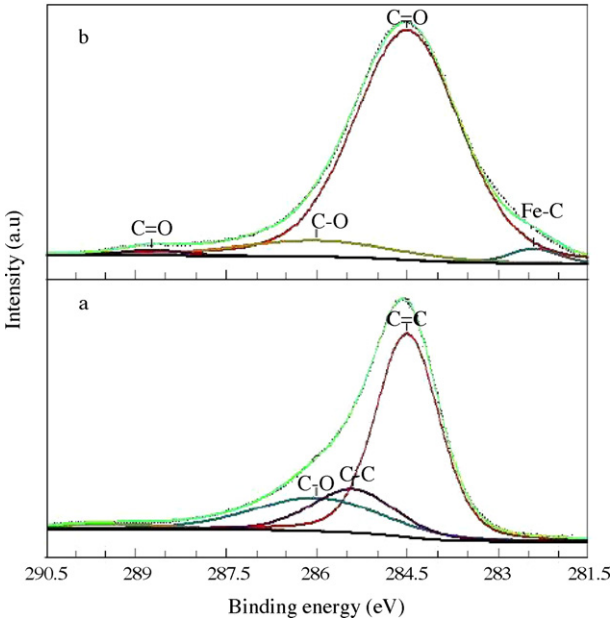

Fig. 4. XPS results of the (a) oxidized and (b) Fe-doped MWCNTs.

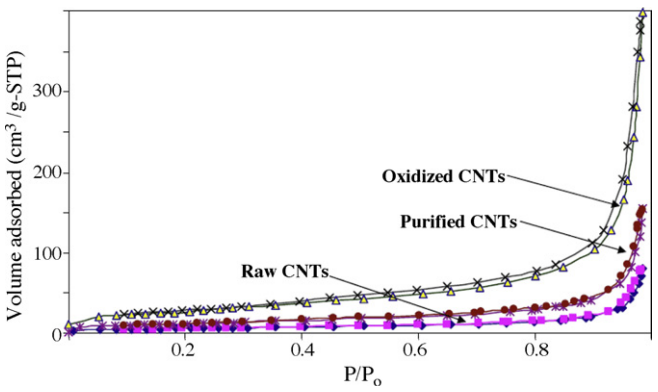

Fig. 5. N_2 adsorption and desorption isotherms of the raw, oxidized and purified MWCNTs.

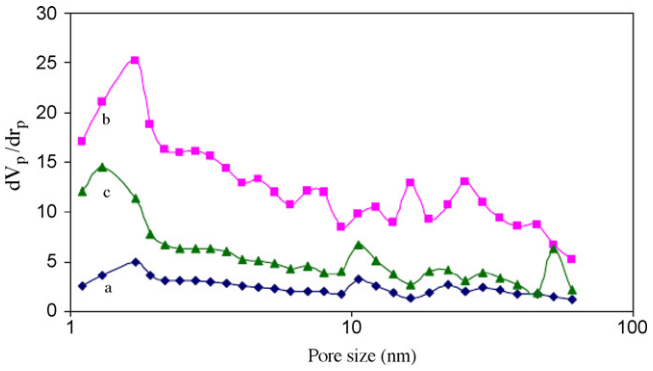

Fig. 6. Pore size distribution of the (a) raw, (b) oxidized and (c) purified MWCNTs.

The XPS results of the oxidized and Fe-doped MWCNTs are shown in Fig. 4 and Table 1. The percentages of the elements existed on the surface of the oxidized and Fe-doped MWCNTs are listed in Table 1. As Table 1 shows, there is no Fe–Ni catalyst on the surface of the oxidized MWCNTs. It can be seen from Fig. 4(a) and (b) that the broad C (1s) peaks of the oxidized and Fe-doped MWCNTs are well-fitted by three and four components, respectively. Fig. 4(a) shows a large peak at 284.5 eV (sp^2 C=C) and two smaller shoulders at around 286 eV (C–O) and 285.4 eV (sp^3 C–C) [13,30,31]. Fig. 4(b) also shows a peak at 284.5 eV (sp^2 C=C) and three smaller shoulders around 288.7 eV (C=O), 286 eV (C–O) and 282.4 eV (Fe–C) [13,30–32]. The XPS results confirmed the formation of C=O hybridization and that sp^3 C–C band disappeared on the surface of MWCNTs by acid treatment. In addition, the existence of Fe–C bands on the surface of MWCNTs is indicative of the attachment of Fe atoms to the surface of MWCNTs.

N_2 adsorption at 77 K is known as a powerful and convenient method to determine the pore size distribution, pore volume and specific surface area of porous materials. Fig. 5 depicts N_2 adsorption isotherms of the raw, oxidized and purified MWCNTs. Adsorption isotherms of the oxidized and purified MWCNTs exhibited an increase in N_2 adsorption below $P/P_o = 0.05$, confirming the existence of the microporous structures in the oxidized and purified MWCNTs [33,34]. The isotherms also indicated adsorption hysteresis behavior of the oxidized and purified MWCNTs in the $P/P_o > 0.3$, due to capillary condensation in the mesopores (Fig. 5). The nitrogen adsorption increased sharply within the pressure range of $P/P_o = 0.9$–0.99, because of the increased adsorption in the intertubular pores [34].

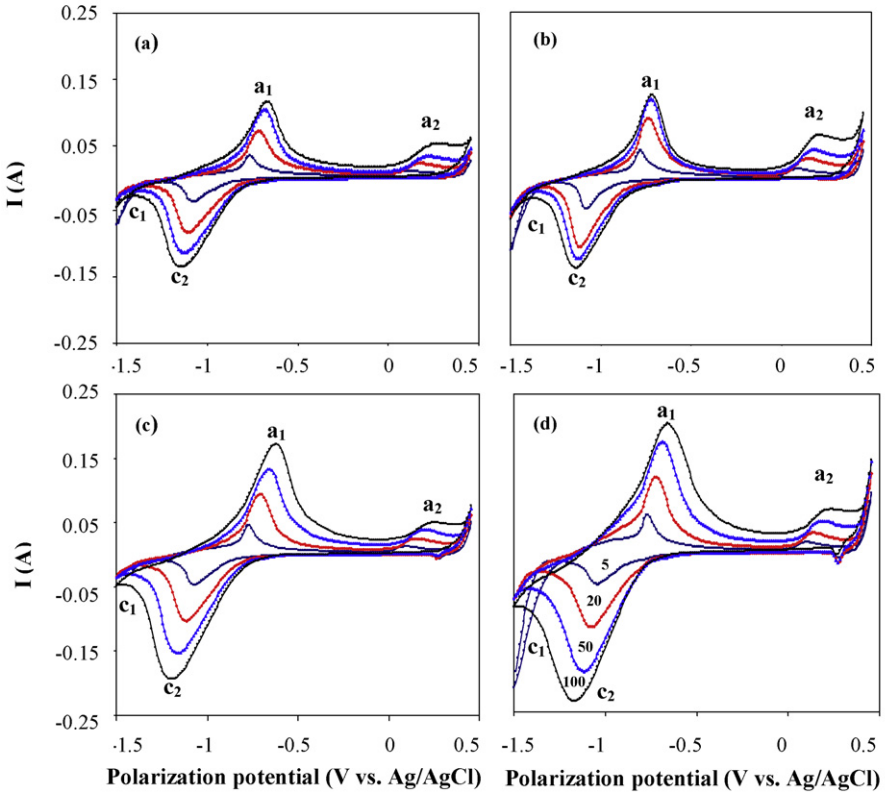

Fig. 7. Cyclic voltammograms of the (a) raw, (b) oxidized, (c) purified and (d) Fe-doped MWCNT electrodes at different sweep rates of 5, 20, 50 and 100 mv s^{-1}.

Table 2
Surface characterizations of the raw, oxidized and purified MWCNTs determined by nitrogen physisorption at 77 K.

MWCNT samples	BET surface area ($m^2\ g^{-1}$)	Total pore volume ($cm^3\ g^{-1}$)	Peak pore size (nm)
Raw	20.1	0.12	1.75
Oxidized	91.7	0.61	1.7
Purified	39.4	0.24	1.3

Fig. 6 shows the porous structures (BJH) of the raw, oxidized and purified MWCNTs. The major peaks of the raw, oxidized and purified MWCNTs were at around 1.75, 1.7 and 1.3 nm, respectively. There was a small peak at around 50 nm for the purified MWCNTs (Fig. 6), probably due to removal of the metal nanoparticles existing in the tips of the MWCNTs by acid treatment.

Surface characterizations of the MWCNTs based on the N_2 adsorption isotherms are summarized in Table 2. The oxidized MWCNTs exhibited a higher specific surface area and pore volume as compared to the raw and purified MWCNT samples. The same results have been reported by Chen et al. [33] for the MWCNTs grown by La-Ni catalyst.

3.2. Hydrogen storage

It is well known that cyclic voltammetry has a high potential to determine the reaction mechanism of redox behaviors. Thus, electrochemical characteristics of the raw, oxidized, purified and Fe-doped MWCNTs were studied by cyclic voltammetry over the potential range of −1.5 to 0.5 V. Fig. 7 indicates the cyclic voltammograms of the raw, oxidized, purified and Fe-doped MWCNT electrodes in various sweep rates.

All the electrodes showed an anodic peak (a_1) around −0.75 V at the sweep rate of 20 mv s^{-1}, corresponding to the oxidation of both Fe to Fe (II) and Fe(II) to Fe(III). Upon the reversal of the scan direction, a corresponding reduction peak (c_2) appeared at around −1.05 V, attributed to the reduction of Fe(II) to Fe and Fe(III) to Fe(II). A similar phenomenon has also been reported by Hang et al. [35] for Fe_2O_3-loaded carbons. Fig. 7 indicates that the Fe-doped MWCNT electrode has the highest peak currents (a_1, c_2) compared to the other MWCNT electrodes. Moreover, the purified MWCNT electrode has higher peak currents as compared with the raw and oxidized MWCNT electrodes due to disappearance of Fe_3C phases resulted in the increasing of Fe interaction with the electrolyte (Fig. 3). The results also showed that by removing of the defective graphite sheets from the raw MWCNTs after annealing at 450 °C in O_2 ambient, their Fe peak currents increased compared to the raw MWCNTs (Fig. 7).

The cyclic voltammetry also indicated that two small peak currents appeared around the potentials of 0.28 and 0.4 V (Fig. 7(c) and (d)), originated from the transformations of Ni(III) to Ni(II) and Ni(II) to Ni(III), respectively [36]. Further, reduction (c_2) and oxidation (a_2) peaks also appeared at about −1.25 and 0.15 V for all the samples. Lombardi et al. reported that these peaks are attributed to hydrogen adsorption/desorption on the surface of MWCNTs [18]. We also observed these peaks in previous work [37] but for detailed investigation, narrower potential ranges were applied for the Fe-doped MWCNT electrode (Fig. 8).

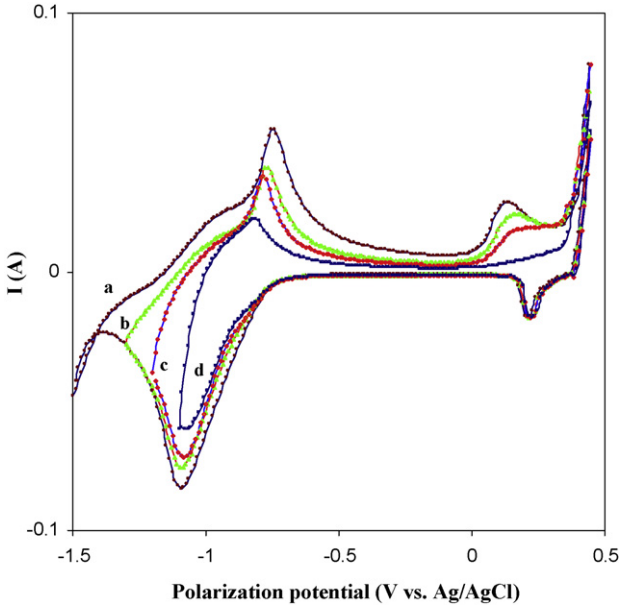

Fig. 8. Cyclic voltammograms of the Fe-doped MWCNT electrode over the potential ranges of (a) −1.5 to 0.5, (b) −1.35 to 0.5, (c) −1.2 to 0.5 and (d) −1.05 to 0.5 V at a sweep rate of 20 mv s^{-1}.

When a narrower potential range was used, the oxidation peak (a_2) decreased and finally the a_2 peak in the potential range of −1.05 to 0.5 V completely disappeared. Hence, it can be concluded that the anodic peak was related to the oxidation of the adsorbed hydrogen. All the results obtained from the cyclic voltammetry and discharge studies are summarized in Table 3.

As shown in Fig. 7 and Table 3, Fe-doped MWCNTs have the highest hydrogen storage capacity among the other MWCNT samples. This result reveals that Fe is an effective catalyst for hydrogen storage (Eq. (1)). Accordingly, the overall reaction mechanism of the MWCNT electrodes can be obtained as follows [2]:

$$H_2O + e^- + M \xrightarrow{RDS} M * H_{ad} + OH^- \quad (1)$$

$$M * H_{ad} + C \rightleftarrows C * H_{ad} + M \quad (2)$$

$$Fe + 2OH^- \rightleftarrows Fe(OH)_2 + 2e^- \quad (3)$$

$$Fe(OH)_2 + OH^- \rightleftarrows Fe(OOH) + H_2O \quad (4)$$

$$Ni(OH)_2 + OH^- \rightleftarrows Ni(OOH) + H_2O \quad (5)$$

The oxidized MWCNT electrode had higher hydrogen storage capacity than the raw MWCNT electrode. Thus, oxidation increased the surface area of MWCNTs. This result was also confirmed by our BET and BJH analyses. As Fig. 7 shows, the peak current of hydrogen adsorption (decomposition of H_2O) increases proportional to the active surface of Fe nanoparticles. Therefore, based on the proposed reaction mechanism, the H_2O decomposition reaction (Eq. (1)) is

Table 3
Electrochemical hydrogen storage data of the raw, oxidized, purified and Fe-doped MWCNTs.

MWCNT samples	Hydrogen storage capacity (C) at different sweep rates (mv s^{-1})						Discharge capacity (mAh g^{-1})
	5	10	20	30	50	100	
Raw	0.18	0.13	0.09	0.06	0.04	0.02	290
Oxidized	0.24	0.17	0.12	0.09	0.06	0.04	340
Purified	0.2	0.13	0.09	0.08	0.05	0.05	345
Fe-doped	0.27	0.2	0.12	0.09	0.06	0.05	510

the rate-determining step (RDS). This result has also been reported by other researchers [17,2].

4. Conclusions

The effects of oxidized, purified and Fe-doped MWCNTs on the hydrogen storage capacity and peak currents of hydrogen adsorption/desorption were studied. The results showed that under similar sweep rates of cyclic voltammetry, the Fe-doped MWCNTs had the highest hydrogen storage capacity as compared to the raw, oxidized and purified MWCNTs. On the other hand, according to the electrochemical observations, with the increase in surface of the catalyst (disappearing of Fe_3C phase), the adsorption/desorption peak currents of hydrogen increased. Electrochemical analyses also showed that H_2O decomposition on the Fe catalyst is the RDS of the hydrogen storage process in the MWCNTs.

Acknowledgements

The authors would like to thank the Research Council of Sharif University of Technology for financial support. The assistances of Mr. M. Asgari and Ms. S. Mirershadi during the various stages of the project and also Dr. Akhavan for useful discussions are greatly acknowledged.

References

[1] K.M. Thomas, Catal. Today 120 (2007) 389.
[2] R. Strobel, J. Garche, P.T. Moseley, L. Jorissen, G. Wolf, J. Power Sources 159 (2006) 781.
[3] Z. Li, Renew Sust. Energy Rev. 9 (2005) 395.
[4] G. Hermosilla-Lara, G. Momen, P.H. Marty, B.L. Neidre, K. Hassouni, Int. J. Hydrogen Energy 32 (2007) 1542.
[5] C.Z. Wu, P. Wang, X. Yao, C. Liu, D.M. Chen, G.Q. Lu, H.M. Cheng, J. Alloys Compd. 420 (2006) 278.
[6] A.C. Dillon, K.M. Jones, T.A. Bekkedahl, C.H. Kiang, D.S. Bethune, M.J. Heben, Nature 386 (1997) 377.
[7] A.K.M. Fazle Kibria, Y.H. Mo, K.S. Nahm, M.H. Yum, Int. J. Hydrogen Energy 26 (2001) 823.
[8] M. Marella, M. Tomaselli, Carbon 44 (2006) 1404.
[9] G. Mpourmpakis, G.E. Froudakis, G.P. Lithoxoos, J. Samios, J. Chem. Phys. 126 (2007) 144704.
[10] X. Chen, Y. Zhang, X.P. Gao, G.L. Pan, X.Y. Jiang, J. Qu, F. Wu, J. Yan, D.Y. Song, Int. J. Hydrogen Energy 29 (2004) 743.
[11] H. Zhang, X. Fu, J. Yin, C. Zhou, Y. Chen, M. Li, A. Wei, Phys. Lett. A 399 (2005) 370.
[12] P. Benard, R. Chahine, Scripta Mater. 56 (2007) 803.
[13] D.Y. Kim, C.M. Yang, H. Noguchi, M. Yamamoto, T. Ohba, H. Kanoh, K. Kaneko, Carbon 46 (2008) 611.
[14] S. Dag, Y. Ozturk, S. Ciraci, T. Yildirim, Phys. Rev. B 72 (2005) 155404.
[15] S. Yi, H. Zhang, L. Pei, Y. Zhu, X. Chen, X. Xue, J. Alloys Compd. 420 (2006) 312.
[16] H. Feng, Y.I. Wei, C. Shao, Y. Lai, S. Feng, Z. Dong, Int. J. Hydrogen Energy 32 (2007) 1294.
[17] C.T. Hsieh, Y.W. Chou, J.Y. Lin, Int. J. Hydrogen Energy 32 (2007) 3457.
[18] I. Lombardi, M. Bestetti, C. Mazzocchia, L. Cavallotti, U. Ducati, Eletrochem. Solid-State Lett. 7 (5) (2004) A115.
[19] T. Tsoufis, P. Xidas, L. Jankovic, D. Gournis, A. Saranti, T. Bakas, M.A. Karakassid, Diamond Relat. Mater. 16 (2007) 155.
[20] N. Lei, K. Keiji, Z. Ling-Ping, K. Tokushi, O. Keishin, M. Kiyaoto, N. Junji, Carbon 44 (2006) 2265.
[21] S.Z. Mortazavi, A. Reyhani, A. Iraji zad, Appl. Surf. Sci. 254 (2008) 6416.
[22] A.K.M. Fazle Kibria, Y.H. Mo, K.S. Nahm, M.J. Kim, Carbon 40 (2002) 1241.
[23] I.O. Hiro-aki, H. Na-oki, Y. Yasuzumi, M. Takanaori, S. Toshimitsu, Diamond Relat. Mater. 16 (2007) 1121.
[24] V.Z. Mordkovich, E.A. Dolgova, A.R. Karaeva, D.N. Kharitonov, I.A. Maslov, A.A. Kamenev, V.F. Tretjakov, Carbon 45 (2007) 62.
[25] C.M. Chen, Y.M. Dai, J.G. Huang, J.M. Jehng, Carbon 44 (2006) 1808.
[26] A. Reyhani, S.Z. Mortazavi, O. Akhavan, A.Z. Moshfegh, Sh. Lahooti, Appl. Surf. Sci. 253 (2007) 8458.
[27] M.S. Dresselhaus, G. Dresselhaus, A. Jorio, F. Souza, Carbon 40 (2002) 2043.
[28] A. Jorio, M.A. Pimenta, A.G. Souza Filho, R. Saito, G. Dresselhaus, S. Dresselhaus, New J. Phys. 5 (2003) 139.1.
[29] E. Yoo, T. Komatsu, N. Yagai, K. Arai, T. Yamazaki, K. Matsuishi, T. Matsumoto, J. Nakamura, J. Phys. Chem. B 108 (2004) 18903.
[30] M. Tan, J. Zhu, J. Han, L. Niu, J. Lu, W. Chen, Mater. Res. Bull. 43 (2008) 1670.
[31] S. Porro, S. Musso, M. Vinante, L. Vanzetti, M. Anderle, F. Trotta, A. Tagliaferro, Physica E 37 (2007) 58.
[32] J. Jiang, T. Feng, X. Cheng, L. Dai, G. Cao, B. Jiang, X. Wang, X. Liu, Sh. Zou, Nucl. Instrum. Methods Phys. Res. B 244 (2006) 327.
[33] M. Chen, H.W. Yu, J.H. Chen, H.S. Koo, Diamond Relat. Mater. 16 (2007) 1110.
[34] Y.Y. Fan, A. Kaufmann, A. Mukasyan, A. Varma, Carbon 44 (2006) 2160.
[35] B.T. Hang, S.H. Yoon, Sh. Okada, J.I. Yamaki, J. Power Sources 168 (2007) 522.
[36] A. Nozad Golikand, M. Asgari, M. Ghannadi Maragheh, S. Shahrokhian, J. Electroanal. Chem. 588 (2006) 155.
[37] A. Reyhani, S.Z. Mortazavi, A. Nozad Golikand, A.Z. Moshfegh, S. Mirershadi, J. Power Sources 183 (2008) 539.